

PACS numbers: 42.25.Dd; 42.62.Be; 42.30.Wb; 87.64.Cc
DOI: 10.1070/QE2004v034n06ABEH002772

Fast path-integration technique in simulation of light propagation through highly scattering objects

A.V. Voronov, E.V. Tret'yakov, V.V. Shuvalov

***Abstract*. Based on the path-integration technique and the Metropolis method, the original calculation scheme is developed for solving the problem of light propagation through highly scattering objects. The elimination of calculations of 'unnecessary' realisations and the phenomenological description of processes of multiple small-angle scattering provided a drastic increase (by nine and more orders of magnitude) in the calculation rate, retaining the specific features of the problem (consideration of spatial inhomogeneities, boundary conditions, etc.). The scheme allows one to verify other fast calculation algorithms and to obtain information required to reconstruct the internal structure of highly scattering objects (of size $\sim$ 1000 scattered lengths and more) by the method of diffusion optical tomography.**

Keywords: *highly scattering media, multiple small-angle scattering, path-integration algorithm, Metropolis method.*

1. Introduction

In recent years, optical tomography (OT) has been extensively developed as a new method for diagnostics of highly scattering objects [1 – 3]. The OT methods assume the possibility of a correct description of propagation of optical radiation in such objects. The complexity of solving this problem, which seems standard at first glance, resulted in the appearance of the independent line of investigations [4 – 8]. Although the description of interaction of radiation with matter is always based on the system of Maxwell's equations, it is impossible to directly use these equations in the case of highly scattering media. The use of statistic methods and correlation functions allows one to pass to the Dyson equation for the mean values and to the Bethe – Salpeter equation for the second moments [9]. However, these equations are not usually solved in practice but are only used to substantiate the passage to the transfer equations, which are now commonly used for solving problems of this type [10 – 12]. In this case, a medium is described by the absorption and scattering coefficients (inverse lengths) and the angular scattering indicatrix [4 – 8].

Because the transfer equations also have no analytic solution in the general case, even simpler models are often used, which are based on some additional assumptions, for example, the diffuse approximation [4 – 8]. Note, however, that the correctness of the latter is questioned [13]. As a rule, a scattering object in these models is described by the same macroscopic characteristics as in transfer equations. The stationary two-flux Kubelka – Munk model [11, 14] and its generalisations [15], and the method of finite elements [16] and integral transformations (in particular, the Melline and Laplace transformations) [17] belong to models of this type. The nonstationary two-flux model [18, 19] retaining a traditional ray ideology also seems rather promising. The results of any approximate calculation are, as a rule, verified by solving numerically the transfer equation [20] or using Monte-Carlo simulations [21 – 24]. In this case, all the basic macroscopic characteristics (statistic properties) describing processes of light propagation are initially incorporated to the model [21].

Unfortunately, when the characteristic size of an object is of the order of 1000 scattering lengths, it is impossible to use the Monte-Carlo method directly because the simulation of 'unnecessary' realisations in this method takes plenty of time. In this case, only $10^{-14} - 10^{-15}$ of a total number of injected photons enters a photodetector aperture, whereas to achieve an accuracy of 1 %, the number of detected photons should be no less than 10^4. At the same time, the diagnostics of namely such objects is the aim of diffusion OT [3 – 6] where the internal structure is reconstructed using the data on spatial distributions of fluxes of detected photons [25 – 27].

In this paper, we describe a new scheme for solving the problem of propagation of light through highly scattering objects, which is based on the path-integration technique and the Metropolis method [28] and allows us to overcome the above-mentioned difficulties. The main advantage of this scheme is a cardinal gain in the calculation time (by 9 – 10 orders of magnitude for objects of size of approximately 1000 scattering lengths). We emphasise that, from the point of view of diffusion OT, this is not simply an increase in the calculation rate but a qualitative breakthrough because such a calculation becomes possible.

The path-integration technique was proposed by Feynman in quantum mechanics [29]. Later, this method was used in problems of propagation of light through turbulence [30, 31]. The path-integration technique was first used to describe multiple scattering by Perelman et al. [32], who, as

A.V. Voronov, E.V. Tret'yakov, V.V. Shuvalov International Teaching and Research Laser Center, M.V. Lomonosov Moscow State University, Vorob'evy gory, 119992 Moscow, Russia

Received 31 December 2003; revision received 20 February 2004
Kvantovaya Elektronika **34** (6) 547 – 553 (2004)
Translated by M.N. Sapozhnikov

other authors later [33, 34], described analytically the average trajectories and second moments. Note that this approach, which is efficient in the case of relatively weak scattering, cannot be used in situations we are interested in. For numerical calculations, the path-integration technique was used for the first time in the model of random walk over a three-dimensional discrete grid [35–37]. The approach described below, which more accurately describes processes of multiple small-angle scattering, better takes into account the role of spatial inhomogeneities, boundary conditions, etc.

2. Definition of the statistical 'weight' of trajectories in terms of their probabilities

As many other authors [4–8], we will not consider here the phase and polarisation of the light field, assuming that their role is insignificant in the case of multiple scattering. Note also that polarisation effects can be rather simply taken into account in the algorithm described below. We will approximate any trajectory of a photon by a series of sufficiently short (with respect to the length of the trajectory itself and all the spatial scales of the problem) linear segments $\Delta\boldsymbol{r}_i = \boldsymbol{r}_{i+1} - \boldsymbol{r}_i$, where $\boldsymbol{r}_i$ is the ith ($i = 1, 2, \ldots, N$) break point of the trajectory. Points $\boldsymbol{r}_1$ and $\boldsymbol{r}_{N+1}$ correspond to the beginning and the end of the trajectory. We describe the spatial orientation of each segment by the azimuthal (θ_i) and polar (φ_i) angles by introducing the corresponding two-dimensional angle $\boldsymbol{\theta}_i = (\theta_i, \varphi_i)$. We assume, as usual, that the probability $P_{ai}(\Delta r_i) = \exp(-\mu_a \Delta r_i)$ of 'successful' (without absorption) passage of a photon through the ith segment is determined only by the segment length $\Delta r_i = |\Delta\boldsymbol{r}_i|$ and the absorption coefficient μ_a, while the scattering probability $P_{si}(\Delta r_i) = 1 - \exp(-\mu_s \Delta r_i)$ is determined by the scattering coefficient (inverse length) μ_s [22].

Let us estimate the probability $P_{si}(\Delta\boldsymbol{\theta}_i, \Delta r_i)$ of a change in the photon propagation direction by the angle $\Delta\boldsymbol{\theta}_i = \boldsymbol{\theta}_{i+1} - \boldsymbol{\theta}_i$ after the photon transition from the segment $\Delta\boldsymbol{r}_i$ to the segment $\Delta\boldsymbol{r}_{i+1}$ on the path Δr_i We assume that each scattering event in a homogeneous medium (in sense of constant values of μ_a and μ_s) is described by the indicatrix $P_s(\Delta\boldsymbol{\theta}, \Delta\boldsymbol{\theta}_s)$, which, in the case of the appropriate normalisation, is simply the distribution of the probability density of scattering over the two-dimensional angle $\Delta\boldsymbol{\theta} = (\Delta\theta, \Delta\varphi)$, having the width $\Delta\boldsymbol{\theta}_s = (\Delta\theta_s, \Delta\varphi_s)$ [11]. Here, $\Delta\theta$ and $\Delta\varphi$ describe changes in the azimuthal and polar propagation angles during scattering. We will estimate the probability $P_{si}(\Delta\boldsymbol{\theta}_i, \Delta r_i)$ taking into account that integration should be performed over all the intermediate directions of propagation on the segment $\Delta\boldsymbol{r}_i$. Therefore, when the probability of a change in the photon propagation direction by the angle $\Delta\boldsymbol{\theta}_i$ in each scattering event is small ($P_s(\Delta\boldsymbol{\theta}, \Delta\boldsymbol{\theta}_s) \ll 1$, small-angle scattering) [11], the probability $P_{si}(\Delta\boldsymbol{\theta}_i, \Delta r_i)$ of rotation by the same angle on the segment Δr_i depends on the number k of scattering events. Strictly speaking, we should introduce the indicatrix for multiple scattering, which can be approximately written as

$$P_{si}(\Delta\boldsymbol{\theta}_i, \Delta r_i) \simeq \sum_{k=0}^{\infty} P^{(k)}(\Delta r_i) P_s^{(k)}(\Delta\boldsymbol{\theta}_i). \tag{1}$$

Here,

$$P^{(k)}(\Delta r_i) \simeq \frac{(\mu_s \Delta r_i)^k}{k!} \exp(-\mu_s \Delta r_i) \tag{2}$$

is the probability of the k-order scattering on the trajectory segment Δr_i, which can be specified by the standard Poisson distribution with the average number of scattering events $\langle k \rangle = N_{si} = \mu_s \Delta r_i$;

$$P_s^{(k)}(\Delta\boldsymbol{\theta}_i) \simeq \int \mathrm{d}\Delta\boldsymbol{\theta}' P_s^{(k-1)}(\Delta\boldsymbol{\theta}') P_s(\Delta\boldsymbol{\theta}_i - \Delta\boldsymbol{\theta}', \Delta\boldsymbol{\theta}_s) \tag{3}$$

is the probability density of the k-order scattering by the angle $\Delta\boldsymbol{\theta}_i$; $P_s^{(0)}(\boldsymbol{\theta}) \equiv \delta(\boldsymbol{\theta})$. Then, the total probability of the photon propagation over each ith segment of the trajectory under study can be written in the form

$$P_i(\Delta\boldsymbol{\theta}_i, \Delta r_i) = \exp(-\mu_a \Delta r_i) P_{si}(\Delta\boldsymbol{\theta}_i, \Delta r_i), \tag{4}$$

and the probability of the photon propagation along the entire trajectory is determined by the expression

$$P(\boldsymbol{r}_1; \ldots; \boldsymbol{r}_i; \ldots; \boldsymbol{r}_{N+1}) = \prod_{i=1}^{N} P_i(\Delta\boldsymbol{\theta}_i, \Delta r_i) = \exp\left(-\mu_a \sum_i \Delta r_i\right) \prod_{i=1}^{N} P_{si}(\Delta\boldsymbol{\theta}_i, \Delta r_i). \tag{5}$$

3. Phenomenological description of multiple scattering processes

It is impossible to calculate all the required angular distributions $P_s^{(k)}(\Delta\boldsymbol{\theta}_i)$ from (3) in the general case. For this reason, approximate calculations can be performed in two different ways. In the first case, all the trajectories are divided into such short segments ($N_{si} = \mu_s \Delta r_i < 1$) that it is sufficient to retain in each segment only two first terms of sum (1) with known angular distributions $P_s^{(0)}(\boldsymbol{\theta}) \equiv \delta(\boldsymbol{\theta})$ ($k = 0$, absence of scattering) and $P_s^{(1)}(\Delta\boldsymbol{\theta}_i) \equiv P_s(\Delta\boldsymbol{\theta}_i, \Delta\boldsymbol{\theta}_s)$ ($k = 1$, single scattering). The rest of the terms in the sum are neglected because $P^{(k)}(\Delta r_i) \ll 1$ for $k \geqslant 2$.

Due to the elimination of simulation of useless realisations (see above), even this simplest approach should provide a considerable advantage in the calculation time compared to standard Monte-Carlo simulations. However, the calculation of propagation of light through a three-dimensional object with the characteristic size of the order of 1000 scattering lengths will remain time consuming. Therefore, we will use an alternative phenomenological approach assuming that the segments, into which trajectories are divided, are sufficiently long ($N_{si} = \mu_s \Delta r_i \gg 1$). We also assume that the angular distribution of the scattering probability on each ith segment remains the same as that for single scattering [$P_{si}(\Delta\boldsymbol{\theta}_i, \Delta r_i) \simeq P_s(\Delta\boldsymbol{\theta}_i, \Delta\boldsymbol{\theta}_{si})$], but its width $\Delta\boldsymbol{\theta}_{si}$ depends now explicitly on Δr_i. The latter assumption looks quite reasonable because the lengths of all segments Δr_i for $\langle k \rangle \gg 1$ become so large that the maximum of the distribution $P^{(k)}(\Delta r_i)$ (2) separates terms with numbers $k \sim N_{si} \gg 1$ from sum (1). The angular distributions of these terms should be rather broad ($\Delta\boldsymbol{\theta}_{si} \gg \Delta\boldsymbol{\theta}_s$) and approximately identical because for $k \sim N_{si} \gg 1$ the consecutive integration in (3) can be performed by treating $P_s(\Delta\boldsymbol{\theta}_i, \Delta\boldsymbol{\theta}_s)$ as the delta function. Therefore, by calculating $P_s(\Delta\boldsymbol{\theta}_i, \Delta r_i)$, we can take out the angular distributions $P^{(k)}(\Delta\boldsymbol{\theta}_i)$ from the sum in (1), which immediately gives

$$P_{si}(\Delta\boldsymbol{\theta}_i, \Delta r_i) \simeq P_s^{(k)}(\Delta\boldsymbol{\theta}_i)\big|_{k=N_{si}} \sum_{k=0}^{\infty} P^{(k)}(\Delta r_i) \equiv$$

$$\equiv P_{\mathrm{s}}^{(k)}(\Delta\boldsymbol{\theta}_i)\big|_{k=N_{si}}. \tag{6}$$

It is this indicatrix of multiple scattering ($k \simeq N_{si}$) (6) that we should find now within the framework of some standard models $P_{\mathrm{s}}^{(k)}(\Delta\boldsymbol{\theta}_i)\big|_{k=N_{si}} \simeq P_{\mathrm{s}}(\Delta\boldsymbol{\theta}_i, \Delta\boldsymbol{\theta}_{si})$.

Although we can perform further calculations for any specific model of the scattering indicatrix, we will use here the Henie–Greenstein model [11] in which $P_{\mathrm{s}}(\Delta\boldsymbol{\theta}, \Delta\boldsymbol{\theta}_{\mathrm{s}})$ is specified by the expression

$$P_{\mathrm{s}}(\Delta\boldsymbol{\theta}, \Delta\boldsymbol{\theta}_{\mathrm{s}}) \equiv P_{\mathrm{s}}^{(g)}(\Delta\boldsymbol{\theta}, g_{\mathrm{s}}) = \frac{1+g_{\mathrm{s}}}{4\pi} \times E^{-1}\left[-\frac{4g_{\mathrm{s}}}{(1-g_{\mathrm{s}})^2}\right] \frac{1-g_{\mathrm{s}}^2}{\left(1+g_{\mathrm{s}}^2-2g_{\mathrm{s}}\cos\Delta\theta\right)^{3/2}}, \tag{7}$$

where $E[x] = \int_0^{\pi/2}(1 - x\sin^2 y)^{1/2}\mathrm{d}y$ is the total normal elliptic Legendre integral of the second kind and $g_{\mathrm{s}} = \langle\cos\Delta\theta\rangle$ is the anisotropy parameter defined as the average cosine of the scattering angle and varying from zero (isotropic scattering) to unity (forward scattering). Expression (7) takes into account the unique relation between $\Delta\boldsymbol{\theta}_{\mathrm{s}}$ and g_{s}, and the two first cofactors in (7) provide the required normalisation of the probability to unity. In the range $1 \geqslant g_{\mathrm{s}} \geqslant 0$, it is convenient to use the approximation

$$E^{-1}\left[-\frac{4g_{\mathrm{s}}}{(1-g_{\mathrm{s}})^2}\right] \simeq \frac{2}{\pi}(1-g_{\mathrm{s}}), \tag{8}$$

which gives finally

$$P_{\mathrm{s}}^{(g)}(\Delta\boldsymbol{\theta}, g_{\mathrm{s}}) = \frac{1}{2\pi^2}\frac{(1-g_{\mathrm{s}}^2)^2}{\left(1+g_{\mathrm{s}}^2-2g_{\mathrm{s}}\cos\Delta\theta\right)^{3/2}}. \tag{9}$$

We will calculate the dependence $g_{si}(\Delta r_i)$ assuming that all the even moments of the distribution of the scattering angle $\Delta\theta$ are 'split' into the products of second-order moments. The relation between the width $\Delta\theta_{\mathrm{s}} \equiv (\langle\Delta\theta^2\rangle)^{1/2}$ of the distribution $P_{\mathrm{s}}^{(g)}(\Delta\boldsymbol{\theta}, g_{\mathrm{s}})$ and the anisotropy parameter g_{s} can be found from the standard expansion

$$g_{\mathrm{s}} = \langle\cos\Delta\theta\rangle = \left\langle\sum_{k=0}^{\infty}(-1)^k\frac{(\Delta\theta^2)^k}{(2k)!}\right\rangle = \sum_{k=0}^{\infty}(-1)^k\frac{\left(\langle\Delta\theta^2\rangle^{1/2}\right)^k}{(2k)!} = \cos(\Delta\theta_{\mathrm{s}}), \tag{10}$$

from which it follows that

$$\Delta\theta_{\mathrm{s}} = \arccos g_{\mathrm{s}}. \tag{11}$$

Because $1 \geqslant g_{\mathrm{s}} \geqslant 0$, the region of variation of $\Delta\theta_{\mathrm{s}}$ should be specified by the relation

$$0 \leqslant \Delta\theta_{\mathrm{s}} \leqslant \frac{\pi}{2}. \tag{12}$$

In the case of small-angle scattering ($g_{\mathrm{s}} \geqslant 0.9$), we can use the approximate equality

$$\Delta\theta_{\mathrm{s}} = [2(1-g_{\mathrm{s}})]^{1/2}. \tag{13}$$

Under the assumption $P_{si}(\Delta\boldsymbol{\theta}_i, \Delta r_i) \simeq P_{\mathrm{s}}(\Delta\boldsymbol{\theta}_i, \Delta\boldsymbol{\theta}_{si})$ that we use here, the relation between $\Delta\theta_{si}$ and the anisotropy parameter g_{si} should be similar to (11),

$$\Delta\theta_{si} = \arccos g_{si}, \quad 1 \geqslant g_{si} \geqslant 0, \quad 0 \leqslant \Delta\theta_{si} \leqslant \frac{\pi}{2}, \tag{14}$$

however, even for $g_{\mathrm{s}} \geqslant 0.9$, scattering is not necessarily small-angle. Taking into account the independence of individual interaction events, it follows from the central limit theorem [38] that for not too long trajectory segments we have

$$\Delta\theta_{si}^2 \simeq N_{si}\Delta\theta_{\mathrm{s}}^2 = \mu_{\mathrm{s}}\Delta r_i\Delta\theta_{\mathrm{s}}^2. \tag{15}$$

At the same time, scattering on long segments should become isotropic [11], and

$$\Delta\theta_{si} \to \frac{\pi}{2} \text{ for } N_{si} = \mu_{\mathrm{s}}\Delta r_i \to \infty. \tag{16}$$

Let us use now a simple interpolating expression

$$\Delta\theta_{si}^2 \simeq \frac{\pi^2}{4}\left[1-\exp\left(-\frac{4}{\pi^2}\,\mu_{\mathrm{s}}\Delta r_i\Delta\theta_{\mathrm{s}}^2\right)\right], \tag{17}$$

which completely satisfies the asymptotics considered above. It follows from (17) that we should use the expression

$$g_{si} \simeq \cos\left\{\frac{\pi}{2}\left[1-\exp\left(-\frac{4}{\pi^2}\,\mu_{\mathrm{s}}\Delta r_i\Delta\theta_{\mathrm{s}}^2\right)\right]^{1/2}\right\}, \tag{18}$$

in all further calculations, and in the case of small-angle scattering of interest to us, we have

$$g_{si} \simeq \cos\left\{\frac{\pi}{2}\left[1-\exp\left(-\frac{8}{\pi^2}\,\mu_{\mathrm{s}}'\Delta r_i\right)\right]^{1/2}\right\}. \tag{19}$$

Here, $\mu_{\mathrm{s}}' = (1-g_{\mathrm{s}})\mu_{\mathrm{s}}$ is the transport scattering coefficient [11]. Taking (6), (9), and (19) into account, we can rewrite expression (5) in the form

$$\begin{aligned} P(\boldsymbol{r}_1;\ldots;\boldsymbol{r}_i;\ldots;\boldsymbol{r}_{N+1}) \simeq{}& \exp\left(-\mu_{\mathrm{a}}\sum_i\Delta r_i\right)\times \\ &\times\prod_{i=1}^{N}\left\{\frac{1}{2\pi^2}\sin^4\left[\frac{\pi}{2}\left[1-\exp\left(-\frac{8}{\pi^2}\,\mu_{\mathrm{s}}'\Delta r_i\right)\right]^{1/2}\right]\right. \\ &\times\left\{1+\cos^2\left[\frac{\pi}{2}\left[1-\exp\left(-\frac{8}{\pi^2}\,\mu_{\mathrm{s}}'\Delta r_i\right)\right]^{1/2}\right]\right. \\ &\left.\left.-2\cos\left[\frac{\pi}{2}\left[1-\exp\left(-\frac{8}{\pi^2}\,\mu_{\mathrm{s}}'\Delta r_i\right)\right]^{1/2}\right]\cos\Delta\theta_i\right\}^{-3/2}\right\}, \end{aligned} \tag{20}$$

which determines within the framework of our model the probability of photon propagation along any trajectory through its break points $\boldsymbol{r}_i$ specified by variables Δr_i and $\Delta\theta_i$.

4. Statistical calculation and mechanical analogy

Obviously, the total probability of photon propagation from a source (point $\boldsymbol{r}_{\mathrm{s}} = \boldsymbol{r}_1$) to a detector (point $\boldsymbol{r}_{\mathrm{d}} = \boldsymbol{r}_{N+1}$) can be now described by the expression

$$P(\boldsymbol{r}_{\mathrm{s}} \to \boldsymbol{r}_{\mathrm{d}}) = \int_V \mathrm{d}\boldsymbol{r}_2\ldots\mathrm{d}\boldsymbol{r}_i\ldots\mathrm{d}\boldsymbol{r}_N P(\boldsymbol{r}_1;\ldots;\boldsymbol{r}_i;\ldots\boldsymbol{r}_{N+1}). \tag{21}$$

Here, integration is performed over the entire phase (configuration) space of the trajectories connecting points $\boldsymbol{r}_s$ and $\boldsymbol{r}_d$, while the probabilities $P(\boldsymbol{r}_1;\ldots;\boldsymbol{r}_i;\ldots\boldsymbol{r}_{N+1})$ of the trajectories are specified by (20). One can easily see that, despite the incoherent nature of a superposition of the 'weights' of the latter (due to multiple scattering), our approach led to the expression that is typical of the Feynman quantum mechanics [29]. The problem is reduced to the calculation of the continual integral (21), this procedure being well developed [39].

Integrals of type (21) in quantum statistics are usually calculated numerically. In this case, an instability often appears which requires the introduction of certain restrictions on the integration region. We assume below that all the trajectory segments are comparatively short and have approximately the same length $[\mu_s^{-1} \ll \Delta r_i \simeq \Delta r_0 < (\mu_s')^{-1}]$, while a total number N of nodes is variable. Taking this into account, after the change of variables

$$\{\boldsymbol{r}_1;\ldots;\boldsymbol{r}_i;\ldots;\boldsymbol{r}_{N+1}\} \underset{\Delta r_i=\Delta r_0}{\longrightarrow} \{\boldsymbol{r}_1,\boldsymbol{\theta}_1;\Delta\boldsymbol{\theta}_1;\ldots;\Delta\boldsymbol{\theta}_i;\ldots;\Delta\boldsymbol{\theta}_N\}, \tag{22}$$

and simple algebraic transformations, expression (21) can be written in the form

$$P(\boldsymbol{r}_s\to\boldsymbol{r}_d)=\int_0^\infty \mathrm{d}N\int \Delta\boldsymbol{\theta}_1\ldots\Delta\boldsymbol{\theta}_i\ldots\Delta\boldsymbol{\theta}_N \tag{23}$$

$$\times P(N;\Delta\boldsymbol{\theta}_1;\ldots;\Delta\boldsymbol{\theta}_i;\ldots;\Delta\boldsymbol{\theta}_N)\delta\left(\boldsymbol{\theta}_{N+1}-\boldsymbol{\theta}_1-\sum_{i=1}^{N}\Delta\boldsymbol{\theta}_i\right),$$

$$P(N;\Delta\boldsymbol{\theta}_1;\ldots;\Delta\boldsymbol{\theta}_i;\ldots;\Delta\boldsymbol{\theta}_N)=\exp\left\{-\frac{\sum_{i=1}^{N}\Delta\theta_i^2}{{}^2\!/_3(\mu_s'\Delta r_0)^2}\right.$$

$$\left.-N\ln\left\{\frac{\pi^2}{2}(\mu_s'\Delta r_0)\left[1+\frac{5}{6}(\mu_s'\Delta r_0)\right]^{3/5}\right\}-N(\mu_a\Delta r_0)\right\}. \tag{24}$$

The delta function appearing in (23) restricts the integration region by a space of connected trajectories ($\boldsymbol{\theta}_{N+1}=\boldsymbol{\theta}_1+\sum_{i=1}^{N}\Delta\boldsymbol{\theta}_i$). Expression (24) was written by retaining several first terms of standard power expansions in (20) and the result was again convoluted to an exponential. The limitation of the phase space is justified only when a photon experiences a sufficiently large and approximately equal number ($N_{si}=\mu_s\Delta r_0 \gg 1$) of scattering events during transitions from one trajectory node to another. If the scattering order is small, interference effects should play a significant role, and the applicability of even standard Monte-Carlo simulations is limited.

One can easily see that, as in the quantum-mechanical problems with a variable number of particles – bosons [39], a total number of integration variables in (23) is not fixed. Within the framework of quantum-mechanical analogy, the first term in the exponent in (24) describes 'the energy of elastic coupling' between the adjacent nodes of the trajectories – 'bosons', while two other terms specify their 'chemical potential'. Note that even in a spatially homogeneous scattering medium (with constant values of μ_a, μ_s, and g_s), these two terms cannot be discarded because a total number of nodes on trajectories 'bosons') can vary. Only when the dispersion of trajectory lengths is comparatively small (the case of weak scattering or consideration of only 'almost' ballistic photons [4–8]), the number N of nodes on trajectories can be considered constant, and further calculations can be reduced to the problem that has been solved by Perelman [32].

Continual integrals of type (23) are usually calculated by statistical methods, for example, by the Metropolis method [28]. In this method, the random Markovian process is constructed in the configuration space $s\in\{s_1,s_2...,s_j,\ldots\}$, where $s_j=\{N_j;\boldsymbol{r}_1;\ldots;\boldsymbol{r}_i;\ldots;\boldsymbol{r}_{N_j+1}\}$. The probability $P(s\to s')$ of transition from one configuration to another is assumed dependent on the initial (s) and final (s') states and is defined so that the distribution $\{s_n\}$ converges to the specified distribution $\pi(s)$. In this case, if the ergodicity and detailed balance conditions are fulfilled

$$\pi(s)P(s\to s')=\pi(s')P(s'\to s), \tag{25}$$

this distribution converges to the equilibrium distribution

$$\sum_s \pi(s)P(s'\to s)=\pi(s'). \tag{26}$$

The transition probability $P(s\to s')$ can be represented as the product

$$P(s\to s')=T(s\to s')A(s\to s'), \tag{27}$$

where $T(s\to s')$ and $A(s\to s')$ are the probabilities of the choice and adoption of the s' state upon transition from the s state. The detailed balance is achieved when

$$A(s\to s')=\min\left\{1,\frac{T(s'\to s)\pi(s')}{T(s\to s')\pi(s)}\right\}. \tag{28}$$

By using the Metropolis method, we assumed that all the nodes are identical and the probability $T(s\to s')$ is independent of their position. In this case, it is sufficient to determine the ratio of probabilities for two trajectories: the old one – $P(\boldsymbol{r}_1;\ldots;\boldsymbol{r}_i;\ldots;\boldsymbol{r}_{N+1})$ (node positions $\{\boldsymbol{r}_1;\ldots;\boldsymbol{r}_i;\ldots;\boldsymbol{r}_{N+1}\}$) and the new one – $P(\boldsymbol{r}_1';\ldots;\boldsymbol{r}_i';\ldots;\boldsymbol{r}_{N+1}')$ (node positions $\{\boldsymbol{r}_1';\ldots;\boldsymbol{r}_i';\ldots;\boldsymbol{r}_{N+1}'\}$). In this procedure, each new trajectory was constructed by modifying the position of one of the nodes of the old trajectory whose number i was selected randomly. Because any node 'interacts' only with two nearest neighbours (24), this ratio can be represented in the first approximation in the form

$$\frac{P(\boldsymbol{r}_1;\ldots;\boldsymbol{r}_{i-1};\boldsymbol{r}_i';\boldsymbol{r}_{i+1};\ldots;\boldsymbol{r}_{N+1})}{P(\boldsymbol{r}_1;\ldots;\boldsymbol{r}_{i-1};\boldsymbol{r}_i;\boldsymbol{r}_{i+1};\ldots;\boldsymbol{r}_{N+1})}$$

$$=\exp\left\{\frac{1}{2}\frac{\Delta r_i+\Delta r_{i-1}}{\Delta r_0}\left\{\frac{\Delta\theta_{i+1}^2+\Delta\theta_i^2+\Delta\theta_{i-1}^2}{{}^2\!/_3(\mu_s'\Delta r_0)^2}\right.\right.$$

$$\left.+2\ln\left[\frac{\pi^2}{2}(\mu_s'\Delta r_0)\left[1+\frac{5}{6}(\mu_s'\Delta r_0)\right]^{3/5}\right]+2\mu_a\Delta r_0\right\}$$

$$-\frac{1}{2}\frac{\Delta r_i'+\Delta r_{i-1}'}{\Delta r_0}\left\{\frac{(\Delta\theta_{i+1}')^2+(\Delta\theta_i')^2+(\Delta\theta_{i-1}')^2}{{}^2\!/_3(\mu_s'\Delta r_0)^2}\right.$$

$$\left.\left.+2\ln\left[\frac{\pi^2}{2}(\mu_s'\Delta r_0)\left[1+\frac{5}{6}(\mu_s'\Delta r_0)\right]^{3/5}\right]+2\mu_a\Delta r_0\right\}\right\}. \tag{29}$$

Here, the prime indicates that the value of the parameter for a new trajectory is substituted.

The position of $\boldsymbol{r}_i$ was varied assuming that the relative changes in the lengths of segments $\Delta\boldsymbol{r}_{i-1}$ and $\Delta\boldsymbol{r}_i$ were small. If the condition $|(\Delta r_i' + \Delta r_{i-1}')(2\Delta r_0)^{-1} - 1| < 0.05$ was violated, the nodes were again uniformly redistributed over a trajectory using its parabolic approximation and (if necessary) the value of N was changed. In this case, both the trajectory curvature and its length remained the same, i.e., its total probability also did not change. In the cases when the inequality

$$\frac{P(\boldsymbol{r}_1;\ldots;\boldsymbol{r}_{i-1};\boldsymbol{r}_i';\boldsymbol{r}_{i+1};\ldots;\boldsymbol{r}_{N+1})}{P(\boldsymbol{r}_1;\ldots;\boldsymbol{r}_{i-1};\boldsymbol{r}_i;\boldsymbol{r}_{i+1};\ldots;\boldsymbol{r}_{N+1})} \geqslant \mathscr{R}$$

was valid ($\mathscr{R}$ is a random number in the interval [0, 1]), according to (28) a new trajectory was 'adopted'. In this case, the photon flux density was renewed $[D(\boldsymbol{r}_i') \to D(\boldsymbol{r}_i') + 1]$ in the vicinity of $\boldsymbol{r}_i'$. In the opposite case

$$\frac{P(\boldsymbol{r}_1;\ldots;\boldsymbol{r}_{i-1};\boldsymbol{r}_i';\boldsymbol{r}_{i+1};\ldots;\boldsymbol{r}_{N+1})}{P(\boldsymbol{r}_1;\ldots;\boldsymbol{r}_{i-1};\boldsymbol{r}_i;\boldsymbol{r}_{i+1};\ldots;\boldsymbol{r}_{N+1})} < \mathscr{R},$$

a new trajectory was 'rejected', and the photon flux density was corrected $[D(\boldsymbol{r}_i') \to D(\boldsymbol{r}_i') + 1]$ already in the vicinity of $\boldsymbol{r}_i$. The size of this vicinity was determined by the memory capacity used for the storage of the array $D(\boldsymbol{r})$, i.e., by the size of cells of the grid on which the required distribution of the photon flux density was mapped.

After the renewal, a new node was again randomly selected on the trajectory, and the modification procedure was repeated for this node. Calculations were performed until the array $D(\boldsymbol{r})$ was described with the required accuracy. Note that, although unlike many other procedures, the grid in the scheme described above is used only for data recording, i.e., for preserving the output distribution $D(\boldsymbol{r})$, the spatial resolution of the algorithm can be improved only by decreasing the cell size and correspondingly increasing the total calculation time at the same statistical error per cell.

The spatial inhomogeneity of the problem (the presence of boundaries, inclusions, etc.) in the algorithm described above can be easily taken into account by introducing spatial modulation (dependence on $\boldsymbol{r}$) of two standard parameters μ_a and μ_s' used in (24) to describe the properties of a scattering medium. Although their dependence on $\boldsymbol{r}$ is specified functionally (continuously) in this case, the consideration of variations in μ_a and μ_s' at spatial scales smaller than Δr_0 is not rational because it leads to a substantial increase in the calculation time. Note also that, according to (24), any perfectly absorbing boundary plays the role of an infinitely high potential barrier for the nodes. This means that, if one of the trajectory nodes passes behind such a barrier during the trajectory modification, then the trajectory probability vanishes and the corresponding realisation should be rejected at once. This leads to certain restrictions. The matter is that a new trajectory in the algorithm described above is always generated due to the modification of the old trajectory. The presence of high potential barriers, which cannot be virtually surmounted in the case of small (see above) changes in the position of only one of the nodes (for example, in the case of highly absorbing inclusions intersecting the entire object), inevitably leads to the division of the configuration space of the trajectories into two (or more) unconnected sets. Because the passage from one set to another is impossible, a part of trajectories are lost. This can be avoided by using more complicated algorithms in the Metropolis method.

One can easily see that the algorithm described above allows one to calculate both distributions and mean values of any parameters important for experiments. In this case, all the mean values are determined by averaging over realisations at fixed points $\boldsymbol{r}_s$ and $\boldsymbol{r}_d$. For example, the mean time $\langle\tau\rangle$ of photon propagation from a radiation source to a detector and the mean length $\langle L\rangle$ of the corresponding trajectories are calculated as

$$\langle\tau\rangle = \frac{1}{c}\langle L\rangle = \frac{\Delta r_0}{c}\langle N\rangle = \frac{\Delta r_0}{cm}\sum_{l=1}^{m} N_l. \tag{30}$$

Here, c is the speed of light in a medium; $\langle N\rangle$ is the average number of segments on the trajectories; m is the total number of realisations in the procedure; and N_l is the number of nodes in the lth realisation of the procedure.

Note also that, after substitution (22), the initial propagation angle $\boldsymbol{\theta}_1$ plays the role of an independent variable. No restrictions were imposed on the values of this angle and the final angle $\boldsymbol{\theta}_{N+1}$ in the procedure described above. Therefore, the above expressions correspond to situations with an isotropic (concerning the angular aperture) source and a similar detector. To take the finiteness of angular apertures into account, one should introduce into (29) either the terms describing the 'elastic' interaction with nodes located in two additional points (outside the object) or introduce into (23) the restrictions on the integration region.

5. Approbation of the calculation algorithm

The results of approbation of the calculation algorithm described above are illustrated in Figs 1–4. Figures 1–3 show the isoline maps of the distributions $I(x,y) = \int_{-\infty}^{\infty} \mathrm{d}z D(\boldsymbol{r})$ for photons recorded with a detector at different geometries of the problem. The distribution $I(x,y)$ was mapped using the linear scale of grey gradation. It was assumed in all the realisations that a highly scattering ($\mu_s = 14\ \mathrm{mm}^{-1}$, $g = 0.9$, and $\mu_s' = 1.4\ \mathrm{mm}^{-1}$) and weakly absorbing ($\mu_a = 0.01\ \mathrm{mm}^{-1}$) medium is located in an infinite (along the z axis) cylinder with perfectly absorbing walls ($\mu_a \to \infty$). The radiation source and the detector were assumed isotropic (see above) and were located in the plane orthogonal to the z axis at the central angles 180° (Figs 1a and 3a) and 90° (Fig. 2a) on the cylinder surface. The cylinder diameter was comparatively small ($2R = 35$ mm), which allowed us to compare our results with the results of similar calculations (Figs 1b, 2b, 3b) performed by the standard Monte-Carlo method. Note, however, that the angular aperture of a radiation source in these calculations [27] was 10°, the receiving area of the detector being 1 mm^2.

One can easily see that distributions obtained by both these methods are quite similar, although the statistics obtained by the Monte-Carlo method for the IBM PC AMD XP-1800 calculation time of about 10 days is obviously insufficient. Figure 3a illustrates the transformation of the distribution $I(x,y)$ when a highly absorbing inclusion ($\mu_a \to \infty$) of the same shape with the diameter $2r = 12$ mm appeared on the cylinder axis. Unfortunately, similar calculations were performed in [27] for somewhat another realisation when a highly absorbing inclusion of diameter $2r = 3$ mm was strongly displaced towards a radiation source (Fig. 3b). Note that, despite the same

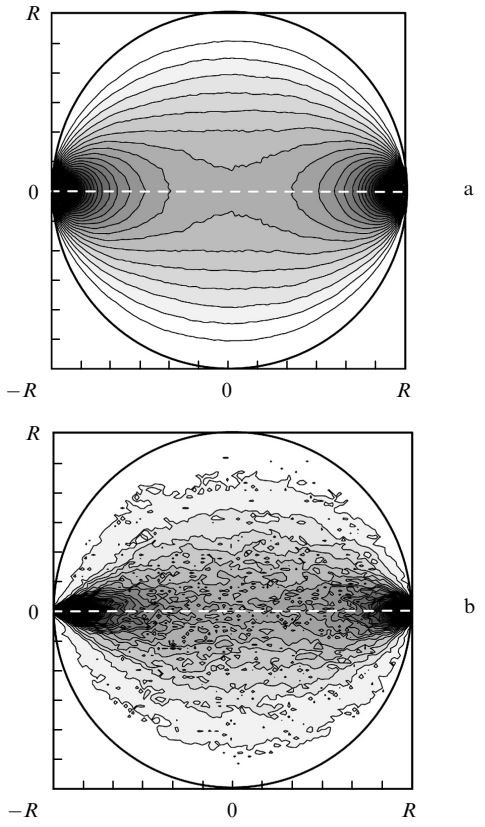

Figure 1. Maps of the distribution $I(x, y)$ in the linear scale of grey gradation for a cylinder with highly absorbing walls obtained using the fast calculation algorithm (a) and Monte-Carlo method (b). The radiation source and detector are located in the plane orthogonal to the z axis at an angle of 180°, $2R = 35$ mm, $\mu_s = 14$ mm^{-1}, $g = 0.9$, $\mu_a = 0.01$ mm^{-1}.

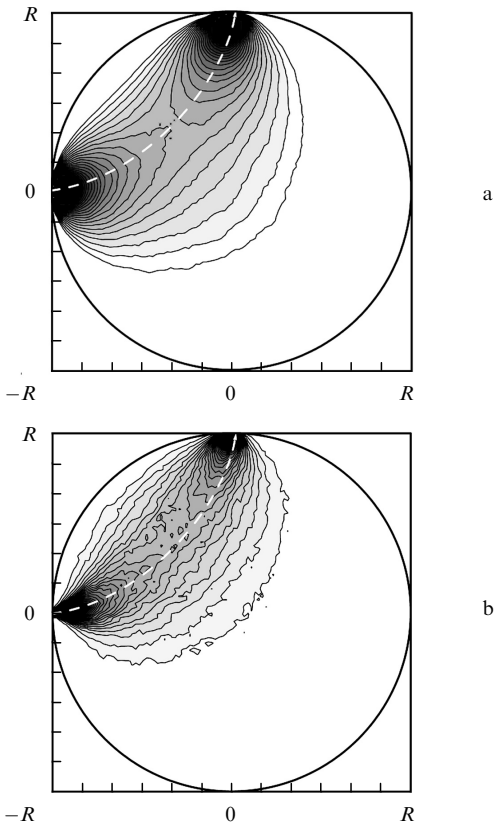

Figure 2. Maps of the distribution $I(x, y)$ in the linear scale of grey gradation for a cylinder with highly absorbing walls obtained using the fast calculation algorithm (a) and Monte-Carlo method (b). The radiation source and detector are located in the plane orthogonal to the z axis at an angle of 90°, $2R = 35$ mm, $\mu_s = 14$ mm^{-1}, $g = 0.9$, $\mu_a = 0.01$ mm^{-1}.

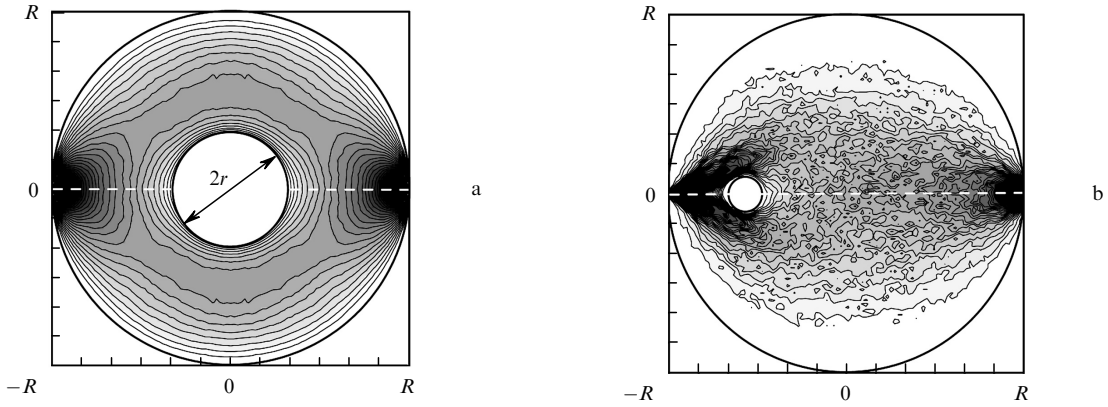

Figure 3. Maps of the distribution $I(x, y)$ in the linear scale of grey gradation for a cylinder with highly absorbing walls and an inclusion obtained using the fast calculation algorithm for $2r = 12$ mm (a) and Monte-Carlo method for $2r = 3$ mm (b). The radiation source and detector are located in the plane orthogonal to the z axis at an angle of 180°, $2R = 35$ mm, $\mu_s = 14$ mm^{-1}, $g = 0.9$, $\mu_a = 0.01$ mm^{-1}.

calculation time (10 days), the statistics obtained by the Monte-Carlo method proves to be in this case even worse than in two previous cases. Figure 4 shows the so-called time-of-flight characteristic calculated using a fast algorithm, i.e., the distribution of the time of flight of photons from the source to the detector. The time axis is normalised to the ballistic (without scattering) time of flight τ_0.

6. Conclusions

We have described the fast algorithm for solving problems of light propagation through highly scattering large objects. The algorithm is based on the path-integration technique and the Metropolis method and excludes, first, the simulation of useless realisations (when a photon was absorbed or missed a photodetector), which increases the calculation rate by six and more orders of magnitude for

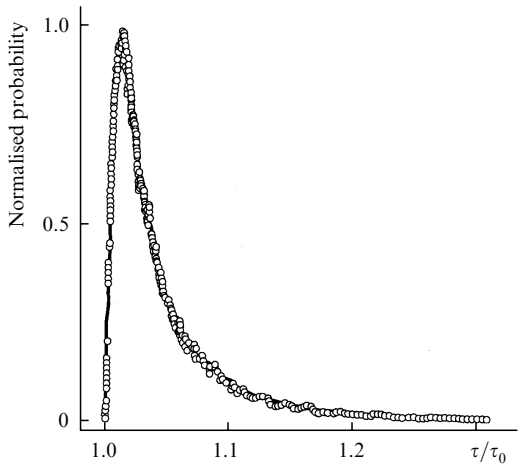

Figure 4. Time-of-flight characteristic calculated using the fast calculation algorithm. The time axis is normalised to the ballistic flight time τ_0 (without scattering).

objects of size ~ 1000 scattering lengths, and, second, drastically reduces (by three orders of magnitude) the calculation time of useful realisations (when a photon was not absorbed and entered a photodetector). The latter is achieved due to a motivated (the central limit theorem) phenomenological description of multiple small-scale scattering. Spatial inhomogeneities, boundary conditions, etc. are taken into account within the framework of standard parameters μ_a and μ_s'. This algorithm can be used to verify other approximate calculation methods, such as the 'mean' trajectory method [33, 34], 'scaling' method [27], etc., and to obtain reliable reference information required for reconstructing the internal structure of highly scattering objects of size ~ 1000 scattering lengths and more in diffusion optical tomography.

Acknowledgements. This work was supported by the Russian Foundation for Basic Research (Grant No. 01-02-17305) and the RF President Program for Supporting the Leading Scientific Schools (Grant No. NSh-1583.2003.2).

References

1. Tuchin V.V. *Usp. Fiz. Nauk*, **167**, 517 (1977); Zimnyakov D.A., Tuchin V.V. *Kvantovaya Elektron.*, **32**, 849 (2002) [*Quantum Electron.*, **32**, 849 (2002)].
2. Minet O., Mueller G.J., Beuthan J. (Eds) *Selected Papers on Optical Tomography: Fundamentals and Applications in Medicine* (Bellingham: SPIE, 1998) Vol. MS-147.
3. Andersson-Engels S., Fujimoto J.G. (Eds) *Photon Migration, Diffuse Spectroscopy, and Optical Coherence Tomography: Imaging and Functional Assessment* (SPIE, 2000) Vol. 4160.
4. Chance B. (Ed.) *Photon Migration in Tissues* (New York: Plenum Press, 1989).
5. Chance B., Delpy D.T., Muller G.J (Eds) *Photon Propogation in Tissues* (SPIE, 1996) Vol. 2626.
6. Benaron D.A., Chance B., Muller G.J. (Eds) *Proc. of Photon Propagation in Tissues II* (SPIE, 1996) Vol. 2925.
7. Benaron D.A., Chance B., Ferrari M. (Eds) *Proc. of Photon Propagation in Tissues III* (SPIE, 1998) Vol. 3194.
8. Benaron D.A. et al. (Eds) *Proc. of Photon Propagation in Tissues IV* (SPIE, 1998) Vol. 3566.
9. Barbanenkov Yu.N. et al. *Usp Fiz. Nauk*, **102**, 3 (1970).
10. Kol'chuzhkin A.M., Uchaikin V.V. *Vvedenie v teoriyu prokhozhdeniya chastits cherez veshchestvo* (Introduction to the Theory of Particle Propagation through Matter) (Moscow: Atomizdat, 1978).
11. Ishimaru A. (Ed.) *Wave Propagation and Scattering in Random Media, Vols 1 and 2* (New York: Academic Press, 1978; Moscow: Mir, 1981).
12. Apresyan L.A., Kravtsov Yu.A. *Teoriya perenosa izlucheniya* (Theory of Radiation Transfer) (Moscow: Nauka, 1983).
13. Tereshchenko S.A. *Izv. Vyssh. Uchebn. Zaved., Ser. Elektron.*, **6**, 101 (1997).
14. Moon J.A., Reinjes J. *Opt. Lett.*, **19**, 521 (1994).
15. Selishchev S.V., Tereshchenko S.A. *Pis'ma Zh. Tekh. Fiz.*, **21**, 24 (1995).
16. Yoon G. et al. *IEEE J. Quantum Electron.*, **QE-23**, 1721 (1987).
17. Arridge S.R., Schweiger M. *Appl. Opt.*, **34**, 8026 (1995).
18. Schweiger M., Arridge S.R. *Appl. Opt.*, **36**, 9042 (1997).
19. Tereshchenko S.A., et al. *Kvantovaya Elektron.*, **23**, 265 (1996) [*Quantum Electron.*, **26**, 258 (1996)].
20. Selishchev S.V., Tereshchenko S.A. *Zh. Tekh. Fiz.*, **67**, 61 (1997).
21. Hielscher A.H., Alcouffe R.E. *Proc. SPIE Int. Soc. Opt. Eng.*, **2925**, 22 (1996).
22. Feng S.C., Zeng F.-A., Chance B. *Proc. SPIE Int. Soc. Opt. Eng.*, **1888**, 78 (1993).
23. Hiraoka M. et al. *Physics in Medicine and Biology*, **38**, 1859 (1993).
24. Pifferi A. et al. *Appl. Opt.*, **37**, 2774 (1998).
25. Savchenko E.P., Tuchin V.V. *Proc. SPIE Int. Soc. Opt. Eng.*, **4001**, 317 (2000).
26. Malikov E.V., Petnikova V.M., Chursin D.A., Shuvalov V.V., Shutov I.V. *Kvantovaya Elektron.*, **30**, 78 (2000) [*Quantum Electron.*, **30**, 78 (2000)].
27. Tret'yakov E.V., Shuvalov V.V., Shutov I.V. *Kvantovaya Elektron.*, **31**, 1095 (2001); **32**, 941 (2002) [*Quantum Electron.*, **31**, 1095 (2001); **32**, 941 (2002)].
28. Metropolis N. et al. *J. Chem. Phys.*, **21**, 1087 (1953).
29. Feynman R.P., Hibbs A.R. *Quantum Mechanics and Path Integrals* (New York: McGraw-Hill Higher Education, 1965).
30. Gross E.P. *J. Math. Phys.*, **24**, 399 (1983).
31. Tessendorf J. *Phys. Rev. A*, **35**, 872 (1987).
32. Perelman L.T. et al. *Phys. Rev. Lett.*, **72**, 1341 (1994).
33. Kravtsenyuk O.V., Lyubimov V.V. *Opt. Spektrosk.*, **88**, 670 (2000).
34. Kalintsev A.G. et al. *Proc. SPIE Int. Soc. Opt. Eng.*, **4242**, 275 (2001).
35. Bonner R.F. et al. *J. Opt. Soc. Am. A*, **4**, 423 (1987).
36. Hebden J.C., Hall D.J., Delpy D.T. *Medical Phys.*, **22**, 201 (1995).
37. Gandjbakhche A.H. et al. *Appl. Opt.*, **37**, 1973 (1998).
38. Akhmanov S.A., D'yakov Yu.E., Chirkin A.S. *Vvedenie v statisticheskuyu radiofiziku i optiku* (Introduction to Statistical Radiophysics and Optics) (Moscow: Nauka, 1981).
39. Kleinert H. *Path Integrals in Quantum Mechanics, Statistics, and Polymer Physics* (Singapore: World Scientific, 1995).